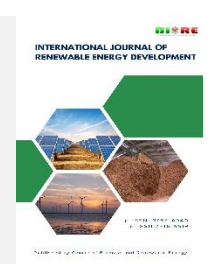


Contents list available at CBIORE journal website

Remarkable Energy Development

Journal homepage: https://ijred.cbiore.id



Research Article

Supercapacitive performance and CO₂ capture capacities of different porous corn stover-derived activated carbons

Oluwashina Philips Gbenebor* o and Abimbola Patricia Idowu Popoola

Department of Chemical, Metallurgical and Materials Engineering, Tshwane University of Technology, Pretoria, South Africa

Abstract. This work focuses on synthesizing activated carbon (AC) from corn wastes from the same plantation – husk (ACH), stalk (ACS), and cob (ACCo). A two-stage pyrolysis (600 °C) with KOH chemical activation was employed. Structural and morphological results from Fourier Transform Infrared spectroscopy (FTIR) and Scanning Electron Microscope (SEM) show that the temperature, concentration, and ratio of biochar-to-KOH solution employed are effective as relevant functional groups and porous structures are formed. The best porous texture is possessed by ACH as N₂ adsorption isotherms result informs that its surface area, pore volume, and size are 904.76 m²/g, 1.00 cm³/g, and 2.09 nm respectively. At 273 K, ACH displays the highest CO₂ adsorption capacity of 4.63 mmolg⁻¹ at 0.95 bar while ACS and ACCo possess CO₂ capture capacities of 3.5 and 3.19 mmolg⁻¹ respectively. Each synthesized AC electrode displays capacitive performance with pseudo capacitance contributions. Dunn and Trasatti analyses show that the capacity of each electrode is more influenced by diffusive contribution. The best porous structure exhibited by ACH is responsible for its superlative electrochemical performance. At current density of 0.5 A/g, its specific capacitance is 430 F/g; this is followed by ACS (257.5 F/g) and the least specific capacitance of 85 F/g is achieved by ACCo. Electrochemical Impedance Spectroscopy (EIS) and Bode plots affirm that with ACH, the fastest diffusion of electrolyte ions into its surface is maintained.

Keywords: CO2 capture, Corn stover, Lignocellulosic biomass, Microporosity, Supercapacitor



@ The author(s). Published by CBIORE. This is an open access article under the CC BY-SA license (http://creativecommons.org/licenses/by-sa/4.0/).

Received: 26th Dec 2024; Revised: 16th July 2025; Accepted: 6th August 2025; Available online: 18th August 2025

1. Introduction

Lignocellulosic biomass is an environmentally friendly renewable resource that has been used to synthesize materials suitable for engineering applications. Aside from the fact that it is a precursor for renewable energy, its availability and being carbon neutral (Luo et al. 2017) make it a preferable material over fossil fuels. Processing techniques such as digestion (Kamperidou & Terzopoulou, 2021; Hashemi et al. 2021; Oliva et al. 2021), pyrolysis (Yu et al. 2022; Fonts et al. 2021), combustion (Blasi, 2009; Carmen & Blasi, 2013; Senneca & Cerciello, 2023), gasification (Alauddin et al. 2010; González et al. 2014), fermentation (Rahmati et al. 2020), etc., have been employed in converting lignocellulose biomass for renewable energy applications. In agriculture, corn stover is regarded as the most abundant biomass residue (waste) among grain crop remnants (Igathinathane et al. 2010) and it comprises leaves, husks, stalks, and cobs that are often discarded after harvest. Among the components of the corn stover, the stalk/stem is confirmed to be the most dominant biomass (Igathinathane et al. 2006). Corn stalk is a major agricultural waste in some nations and has often been converted via pyrolysis to green fuels, which include biochar, biogas, and bio oil (Zeng et al. 2019). The corn husk serves as the ear or shell that protects the maize as it grows. It is often disposed of by burying it in the soil or burning it. According to Reddy & Yang (2015), the husk makes up about 14% of the total corn plant mass, while 50, 23, and 15 % are maintained by the stalk, leaves, and cobs,

respectively. A useful material that can be sourced from this biomass is porous carbon (PC), which includes activated carbon AC (Gan, 2021), graphene (Chen *et al.* 2016), carbon nanotubes (Omoriyekomwan *et al.* 2021), and biochar (Kwapinski *et al.* 2010). Activated carbon has found applications in the areas of energy storage systems (Awasthi *et al.* 2019), heavy metal adsorption (Tounsadi *et al.* 2016), and CO₂ capturing (Serafin *et al.* 2017) owing to its high surface area and complementary electrical conductivity with improved thermal and chemical stability. Corn stalk, husk, and cob wastes have served as a source of this carbonaceous material, with different methods employed in their extraction.

Cao et al. (2016) carbonized pieces of corn stalk core under a nitrogen atmosphere in a muffle furnace at 400 °C for 1 h. The char was mixed with KOH solution, oven-dried (for 24 h), and further activated for 1 h at temperatures ranging between 600-900 °C. The hierarchical pore feature of the char activated at 700 °C was observed to be a combination of micro and mesoporores, which enabled it to exhibit the best capacitive display. Yu et al. (2018) further proved that the corn stalk core can be a good source for supercapacitor electrode material. An optimum temperature of 700 °C (after KOH activation) was reported to engender a porous AC with 2349.89 m²/g surface area with a capacitance of 140 F/g at 1 A/g. Under a nitrogen atmosphere, corn stalk core powder has been carbonized for 5 h at 300 °C in a tubular furnace (Li et al. 2018). A second phase of carbonizing was performed by further heating the sample at

Email: philipsogbenebor@gmail.com (O.P.Gbenebor)

^{*} Corresponding author

550 °C for 4 h. A fraction of the carbonaceous powder was activated in 3 M KOH; this reagent however, created a mesoporous feature with a surface area, pore volume, and average pore size of 393.87 m²g⁻¹, 0.44 cm²g⁻¹ and 8.49 mm respectively. This corn stalk core AC was confirmed suitable for the construction of lithium-ion batteries as its structure effectively permitted the diffusion of lithium ions. In a bid to obtain hierarchical AC suitable for supercapacitors, chemical activation of corn cob derived materials using KOH at 600 °C and 1 h has yielded amorphous carbon having both micro and mesoporous structures (Karnan et al. 2017), feature which was concluded to be responsible for its good performance (as a supercapacitor electrode) in aqueous and ionic liquid electrolytes. It has been reported that the structure of corn husks is lamellar, and KOH plays roles as an exfoliator and creates an array of pores on the biomass (Rani et al. 2020). This was responsible for its large mesoporous volume and specific surface area for supercapacitor electrodes. In their works, sweet corn husk was carbonized in argon atmosphere at 1000 °C and further added to KOH solution in char: KOH ratios of 1:1 and 1:4. Mixtures were dried, and the resultant powder was heated to 800 °C under an argon atmosphere. The researchers observed that both AC samples possessed a similar specific area (1378 m²g⁻¹), which was responsible for their comparable specific capacitance (79 F g-1 at a current density of 1 A g-1). It was thus concluded that the structure of carbon before activation would be responsible for surface area increase and not weight ratio increase.

Different concentrations of KOH solutions of 2, 3, 4, and 5% were used in activating corn stalk powders at 80 °C for 4 h (Zhao *et al.* 2020). The dried samples (after washing) were carbonized at 600 °C under nitrogen flow. Low concentrations of KOH solution produced more micro and mesopores. Increasing the concentration of K₂CO₃ from 1 to 3 M and temperature from 500 to 650 °C has been affirmed to improve the electrochemical storage performance of corn cobs (Olivares *et al.* 2022).

The electrolyte used for the electrochemical study. however, plays a role in the energy storage performance of activated carbon from corn stover. Surya & Michael, (2020) demonstrated this when an electrode synthesized from corn husk AC was exposed to 1 M KCl, 2 M KOH, and 0.5 M H₂SO₄. At a scan rate of 1 mV/s, the electrode in H₂SO₄ possessed the highest specific capacitance (314.83 F/g), followed by KOH (189.57 F/g) and the least (166. 29 F/g), in KCl. Morphological, structural, and electrochemical features of corn husk, cob, fiber, and grains for supercapacitor electrode application have been investigated by Reddygunta et al. (2023). Each precursor was activated with KHCO3 and further carbonized at 900 °C. Using 1 M Na₂SO₄ electrolyte, AC sourced from corn grains had the best electrochemical performance as its porous structure maintained the highest specific surface area of 1804 m²/g. In addition to this, the synthesis culminated in a high graphitization degree coupled with sufficient contents of O and N atoms. These enabled the electrode to possess a specific capacitance of 385 F/g at 0.25 A/g. Optimal parameters recommended for the activation of corn husk to achieve a maximum energy storage performance using K₂CO₂ according to Peralta et al. (2023) was 650 °C pyrolysis temperature and K2CO₃: precursor of 1:2. The synthesis produced a material with amorphous hierarchical pores with heteroatoms containing O, N and S. These heteroatoms were responsible for a specific supercapacitance (269 F/g) from both electrical double layer and faradic contributions. Garcia et al. (2024) activated purple corn cob with varying concentrations of KOH (5, 10, 20, and 30

%), after which pyrolysis (at 700 °C) was carried out. Synthesizing AC using 10 % KOH displayed the highest capacitance and specific capacitance (in 1 mol L⁻¹ H₂SO₄), and this was attributed to the highest microporous surface area (728 m₂/g) which was impacted by the concentration. This optimized parameter also yielded a carbonaceous texture that permitted the diffusion of ions. Mixing carbonized corn husk (600 °C) with KOH in a ratio of 1:2, followed by a further carbonization at 900 °C has culminated in a mesoporous AC with a 1103 m²/g specific surface area (Xiang *et al.* 2024). This was large enough to allow the absorption of electrolyte (1 M KOH), ions which offered additional pseudo capacitance with increased specific capacitance (413.4 F/g).

Various research has proven that diverse properties of AC can be achieved from these common corn stoves through different techniques of physical and chemical activation (or the combination of the two). In this study, the corn stalk, husk, and cob from the same plantation are used for AC synthesis. Porous nature, chemical structure, CO_2 adsorption potency, and electrochemical properties of these carbonaceous materials are investigated and compared.

2. Methodology

2.1. Preparation of activated carbons

Corn cob (CCo), husk (CH), and stalk (CS) were thoroughly washed and sun-dried for 5 days. The dried sets of biomass were pulverized and made to pass through a 250 µm mesh size sieve. The first stage of pyrolysis (to biochar) was carried out by heating each pulverized biomass to 600 °C at 10 °C/min for 1 h in a furnace. At the end of this period, the furnace was switched off, and the biochar was left in the furnace for 24 h. Chemical activation was achieved by mixing each biochar with KOH solution. A gram of biochar was added to 4 g of KOH pellets in 50 ml of distilled water at room temperature. The mixture was thoroughly stirred for 8 h. After this period, the mixture was filtered and the residue was left in the filter paper for 24 h. The second pyrolysis was performed on each KOHrich biochar as earlier done for each biomass. Activated carbon samples were first washed with 1 M HCl (to remove K-rich material), followed by distilled water to neutral pH to eliminate traces of HCl. In this study, activated carbon sourced from corn cob, husk, and stalk is denoted by ACCo, ACH and ACS.

2.2. Characterizations of ACs

Pyrolyzed CH, CS, and CCo with their KOH-activated variants were characterized for their morphological features with the use of a VEGA 3 TESCAN scanning electron microscope (SEM). Functional groups present in pulverized CH, CS, CCo, and their corresponding ACs were deciphered via Fourier Transform Infrared Spectroscopy (FTIR), using a PerkinElmer UATR Two spectrometer. The crystal structure of synthesized ACs was noted using a Philips PW1710 X-Ray diffraction device. With the use of Tristar II 3020, $N_{\rm 2}$ adsorption isotherms were used in determining the porous texture of AC samples at 77K. The CO $_{\rm 2}$ capture capacity of each AC at 273 K was determined with the use of NOVAtouch 2LX. This was performed after each AC was degassed in a vacuum at 300 °C for 48 h.

2.3. Electrode preparation for suparcapacitor

Each AC, carbon black (CB), and Polytetrafluoroethylene (PTFE) was put together in a dish in a controlled mass ratio of 80:10:10. Three drops of N-methylpyrrolidone (NMP) solution were added in steps (a drop per step) to the mixture, after which they were ground with a ceramic laboratory pestle for 30 min. Afterward, the moistened mixture was applied to 1 cm x 1 cm Ni foam and dried at 60 °C in an oven for 12 h. The mass of coated Ni foam before and after drying was measured to be 3 mg.

2.4. Electrochemical measurements

This was carried out in a three-electrode system. In a 6 M KOH electrolyte, the coated Ni foam was the working electrode while Pt wire and Ag/AgCl were used as the counter and reference electrode, respectively. Cyclic voltammetry (CV) and galvanostatic charge-discharge (GCD) tests were measured the electrochemical workstation (AUTOLAB). Frequencies used varied from $10^{-2} - 10^{5}$ Hz with a voltage amplitude of 5 mV. The specific capacitance Cp (derived from the GCD result) was determined using Equation (1) as adopted by Mehdi et al. (2023), Dhineshkumar et al. (2024), and Rajkumar et al. (2024). Furthermore, the GCD also provided the basis for energy density (ED) and power density (PD) calculations as shown in Equations (2) and (3), as employed by Vinayagam et al. (2010).

$$Cp = \frac{I \times \Delta t}{m \times \Delta v} \tag{1}$$

$$ED = \frac{C\Delta V^2}{2 \times 3.6} \tag{2}$$

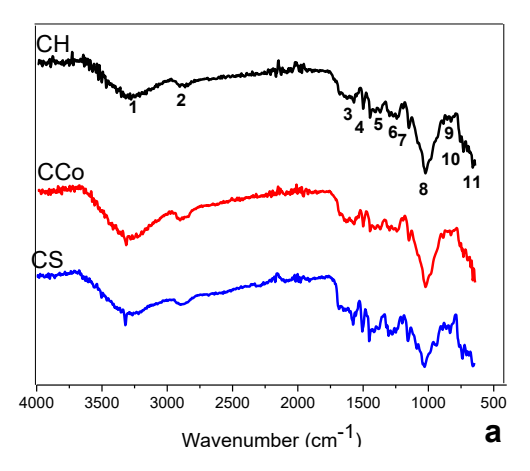
$$PD = \frac{ED \times 3600}{\Delta t}$$
 (3)

The change in time (discharge time) is represented by Δt (s); I is the applied current (A); ΔV represents the potential difference (V), and the mass loading (g) of the electrode material (AC+CB+PTFE) on the Ni foam is denoted by m.

3. Results and discussions

3.1 Functional groups

The FTIR in Figure 1a shows that CH, CCo, and CS contain similar functional groups as listed in Table 1. The spectra patterns are identical, indicating they are from the same stover. In addition, the similarity in spectra patterns is also a



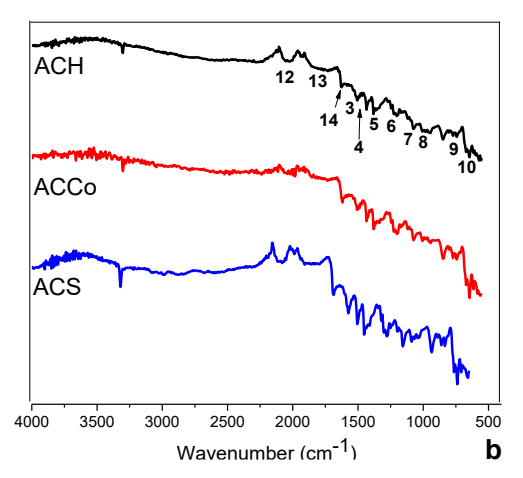


Fig 1. FTIR (a) untreated (b) activated carbon from pulverized CH, CCo and CS (ACH, ACCo, and ACS)

justification that the pulverized corn stovers are lignocellulosic as their functional groups show the existence of cellulose, hemicellulose, and lignin present in other plant biomass (Gbenebor *et al.* 2023). After carbonization by pyrolysis, OH groups in adsorbed water and alcohols, phenols, or carboxylic acid are taken off as illustrated in Figure 1b and Table 1. Furthermore, CH in methyl (CH₃) and methylene groups (CH₂) are eliminated. This explains the processes of dehydration and

Table 1 Functional groups of untreated and activated carbon from pulverized CH, CCo and CS

S/N	Functional groups	СН	CCco	CS	ACH	ACCo	ACS
	OH in adsorbed water and alcohols, phenols or carboxylic						
1	acid	3286	3279	3300			
	Vibrations of CH in methyl and methylene groups						
2	(cellulose, hemicellulose and lignin)	2882	2895	2888			
3	C=C in unsaturated carbon bonds	1592	1578	1578	1571	1571	1571
4	C=C present in aromatic rings		1508	1529	1529	1501	1507
5	C=O, CH in carbonyl and caboxylate groups	1452	1417	1415	1438	1445	1452
6	CO stretching in acetyl groups	1257	1250	1255	1276	1285	1285
7	Anti-symmetric CO-C stretching	1174	1160	1153	1153	1160	1148
8	Vibration of C-O in alcohol, esters, phenols and acids		1020	1027	1034	1034	1055
9	Vibration of CH		815	846	825	825	853
10	Vibration of CH	767	760	748	720	720	741
11	OH vibrations	727	731	731			
12	Stretching of C=N				2094	2094	2087
13	Stretching of CO				1794	1761	1835
14	Stretching of C=O	-			1794	1689	1835

oxidation that often occur during carbonization by pyrolysis; here, CO_2 , CO, and H_2O are given off (Fagbayigbo *et al.* 2017; Mopoung & Dejang, 2021).

3.2. Morphology

The SEM image of CH shown in Figure 2a displays a rough folded-like surface with different geometries of particles lumped in layers. After the first pyrolysis, particles cluster to form a spongy-like structure with a shiny surface (Figure 2b). This could be ascribed to the decomposition of hemicellulose, lignin, cellulose, and some volatile constituents that occurred in CH during the thermal treatment. The second phase of carbonization after room temperature reaction with KOH (ACH) results in a rough broken filiform structure (Figure 2c). The formation of pores in the particles shows a successful KOH activation process. The surface of CS particles appears nearly fiber-like with some degree of partial smoothness (Figure 2d). The fiber-like structure looks more discontinuous and rough after pyrolysis (Figure 2e), showing the effects of dehydration during this process. The lumping of the fiber-like particles observed in Figure 2d is disjointed in Figure 2e with conspicuous area reduction, which explains the complete

degradation of polysaccharides present in CS. Pores are formed throughout the ACS particle surface which appear globular and spongy (Figure 2f). The surface of CCo is characterized by smooth humps and blister-like interactions of cellulose, hemicellulose, and lignin (Figure 2g). These polysaccharides are disintegrated after pyrolysis and the smooth hump surface before the process transforms to carbon-rich fiber-like structures of unequal lengths (Figure 2h). The surface texture of ACCo shows the existence of well-structured pores of non-uniform shapes (Figure 2i). The particle geometry still maintains the fiber-like shape as observed in Figure 2h, but there are some discontinuities on the surface.

3.3. X-Ray Diffraction of ACs

Figure 3 shows the XRD patterns (normalized) of processed ACs with each having two distinct broad peaks as displayed by other biomass-sourced ACs (Vinayagam *et al.* 2020; Vinayagam *et al.* 2021; Hepsiba *et al.* 2022; Vinayagam *et al.* 2024). Each material possesses a stronger peak that is diffracted on $2\theta = 24^{\circ}$, representing the (002) plane. A weaker and broader peak, which represents (100) plane diffraction occurs at $2\theta = 44^{\circ}$, It has been

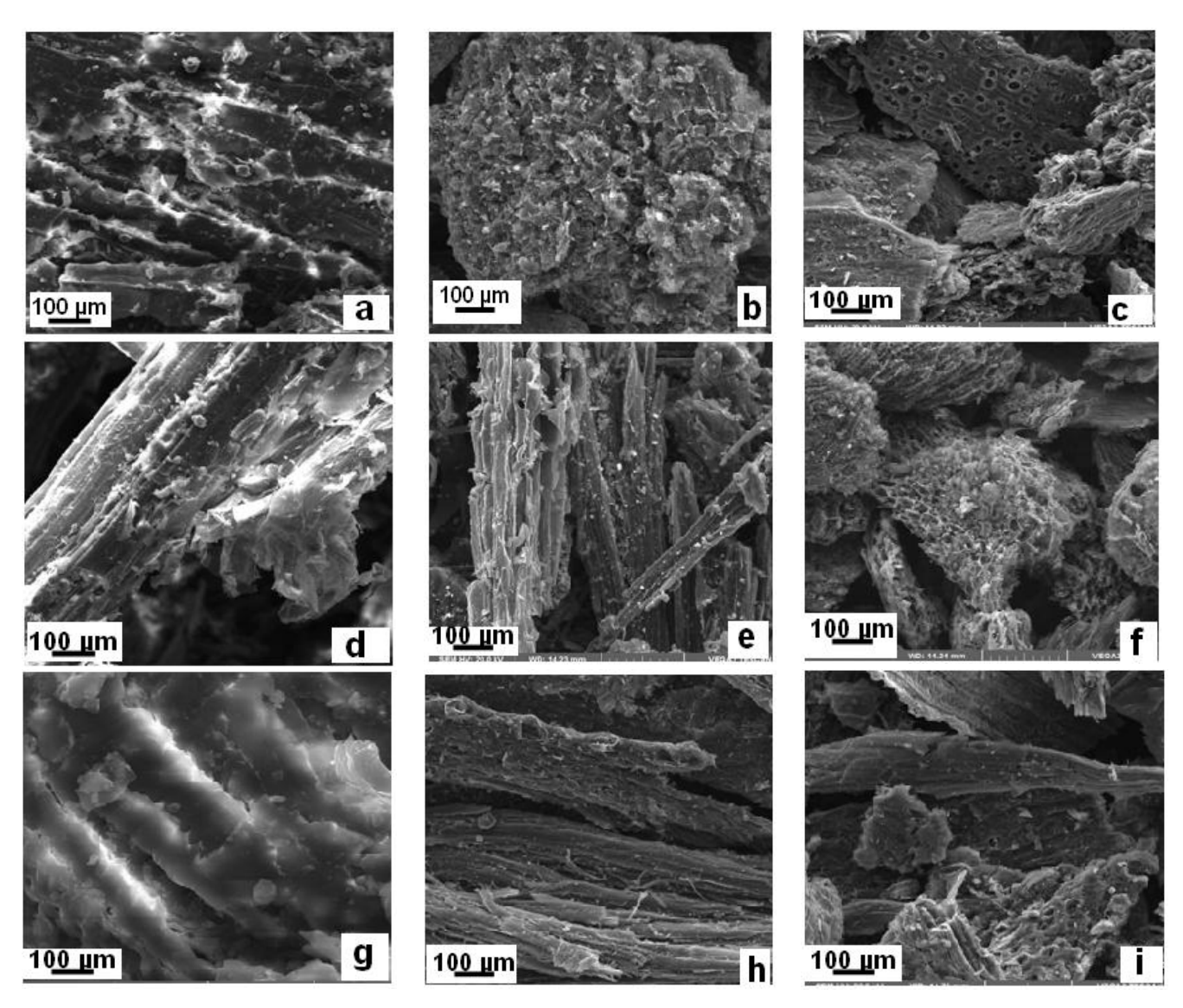


Fig 2 SEM images of (a) CH (b) pyrolized CH (c) ACH (d) CS (e) pyrolized CS (f) ACS (g) CCo (h) pyrolized CCo (i) ACCo

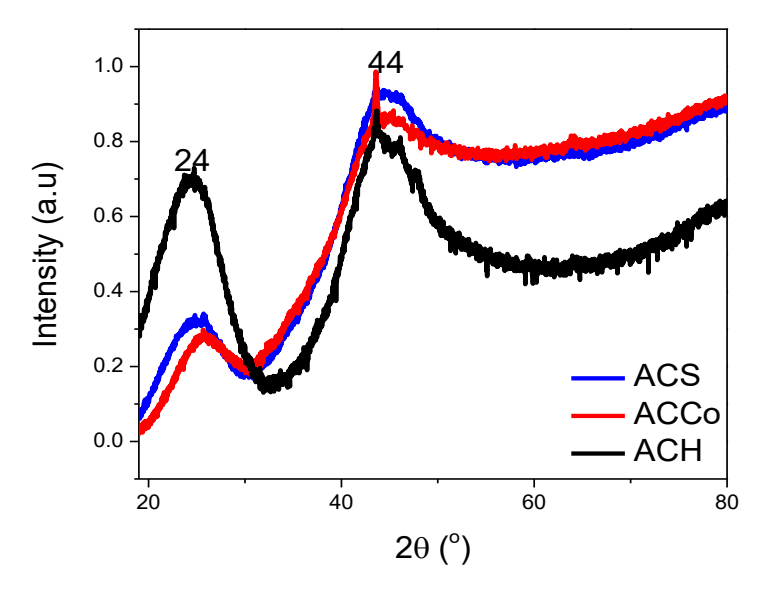


Fig 3. XRD patterns of ACS, ACCo and ACH

reported that these two peaks are graphitic. The diffractogram shows that each material is fully carbonaceous, having these two peaks that depict amorphous structure characteristics comparable to ACs processed from barley straw (Jeloo *et al.* 2024).

3.4. Pore textural properties and CO2 capture capacities

The N_2 sorption isotherms shown in Figure 4 for synthesized ACs are characteristics of the type I model according to the IUPAC classification, as they are devoid of a hysteresis loop.

The ACs are microporous in nature and they can adsorb high quantities of N_2 at relatively low pressures and 77 K. The Figure shows that the quantity of N_2 adsorbed increases with an increase in pressure; ACH possesses the highest BET surface area (S_{BET}), pore size, and volume followed by ACS (Table 2); this confirms that considering constant activation temperature and KOH concentration, biomass type/source is a parameter that influences the porous features of ACs. At a very low relative pressure (below 0.01), there exists a sharp increase in N_2 adsorption, which confirms that the microporosity of ACS, ACCo, and, ACH are made up of ultrafine micropores. The

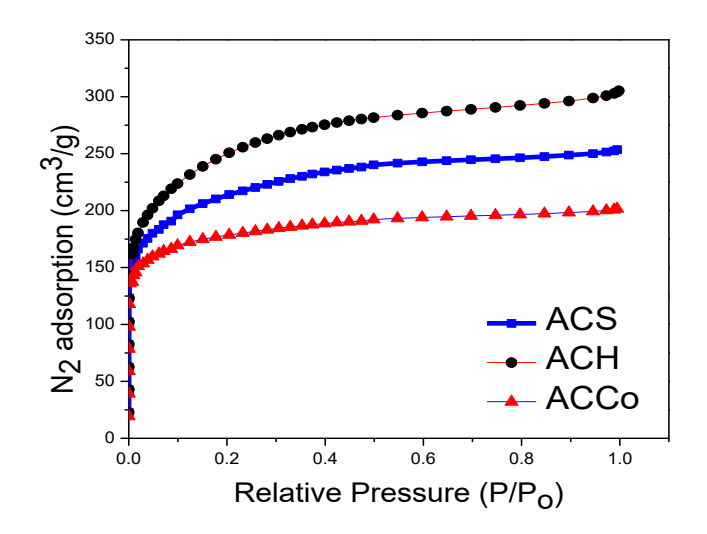


Fig 4. N2 adsorption isotherm for ACS, ACH, and ACCo at 77 K

Table 2Textural properties of ACH, ACCo and ACSS

S/N	Samples	S_{BET} (m ² /g)	Pore volume (cm³/g)	Pore size (nm)
1	ACH	904.76	1.00	2.09
2	ACCo	663.17	0.31	1.88
3	ACS	761.89	0.39	2.06

varying pore textural properties shown in Table 2 justify the role of KOH on each biomass as a dehydrating agent that triggers the opening of pores in biomass. This has created a pore of the largest surface area, volume, and size (diameter) of 904.76 $\rm m^2/g$, 1.00 $\rm cm^3/g$, and 2.09 nm respectively, possessed by ACH. The diameter of $\rm N_2$ molecules is 0.32 nm; hence, most of its molecules will be adsorbed by a structure with a 2.09 nm diameter (possessed by ACH), followed by 2.06 nm maintained by ACS and the least (1.88 nm), exhibited by ACCo. During activation, it has been reported that KOH uses up some carbon in the biomass to engender the formation of pores for adsorption according to the following redox reactions (Rani *et al.* 2020).

$$6KOH + 2C \rightarrow 2K + 3H_2 + 2K_2CO_3$$
 (i)

$$K_2CO_3 \rightarrow K_2O + CO_2$$
 (ii)

$$CO_2 + C \rightarrow 2CO$$
 (iii)

$$K_2CO_3 + 2C \rightarrow 2K+3CO$$
 (iv)

$$C + K_2O \rightarrow 2K + CO$$
 (v)

Figure 5 shows the CO2 adsorption isotherms of the selected corn stover ACs investigated at 273K and 1 bar. It can be

observed that ACH displays the highest CO2 adsorption capacity of 4.63 mmolg-1 at 0.95 bar. Under the same adsorption conditions, ACS and ACCo possess CO2 capture capacities of 3.5 and 3.19 mmolg-1 respectively. The SBET surface area of most porous materials imparts a positive influence on their CO2 adsorption capability and it can therefore be concluded that the highest magnitude of SBET exhibited by ACH (Table 2) is responsible for its superlative CO₂ adsorption performance among the three ACs. Functional group modifications (on the surface) with improved micropore volume which occur after KOH activation have also been reported to enhance CO₂ adsorption capacity of ACs (Singh et al. 2017). This shows that the activation of each biomass with KOH has effectively altered its textural and chemical composition, with the CH displaying the best response. The CO2 adsorption capacities of some other biomass-sourced ACs are presented in Table 3. It should be noted that ACH possesses the highest CO₂ capture capacity among the ones listed even though it has a lower S_{BET} compared to some AC produced from other biomasses. This implies that aside from varying processing parameters observed during AC production, biomass source also plays a key role; the textural property of a particular biomass AC will not function directly for AC from another biomass source during application. The essence of the table is

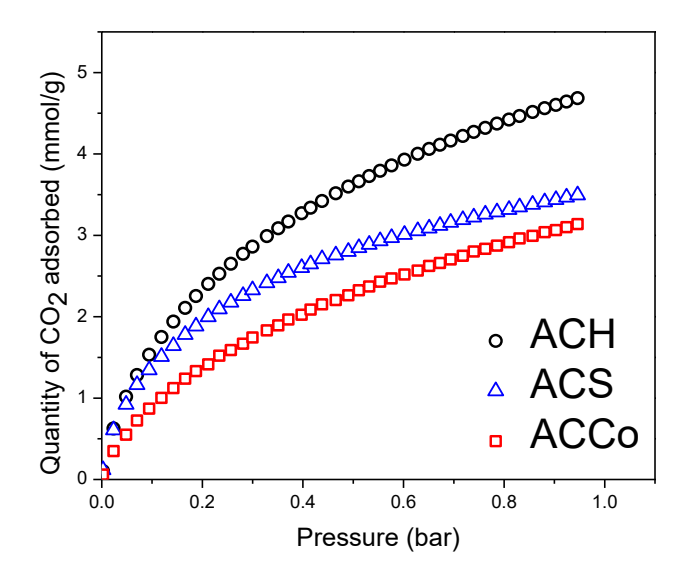


Fig 5. CO2 adsorption isotherm for ACs, ACH and ACCo at 273 K

Table 3 Comparison of CO_2 capture capacities of ACs sourced from different lignocellulosic biomass via pyrolysis and chemical activation with AC synthesized from this study.

Biomass	Activation agent	S_{BET} (m ² /g)	CO ₂ (mmol/g) at 273 K	Ref.
Fern leaves	KOH at 700 °C	1593	4.52	(Serafin et al. 2017)
Arundo donax	KOH at 600 °C	849	3.7	(Singh et al. 2017)
Pristine gelatin	KOH at 700 °C	1294	4.25	(Alabadi <i>et al.</i> 2015)
Starch	KOH at 700 °C	714	3.02	(Alabadi <i>et al.</i> 2015)
Slash pine wood	KOH at 580 °C	979	4.26	(Ahmed et al. 2019)
Walnut shells	KOH at 600 °C	588	1.83	(Pu et al. 2021)
Pomegranate peels	KOH at 700 °C	710	3.9	(Mumtaz et al. 2021)
Lumpy bracket	KOH at 600 °C	483	4.39	(Serafin et al. 2019)
	KOH at 650 °C	559	4.57	(Serafin et al. 2019)
Corn husk	KOH at 600 °C	904.76	4.63	This work
Corn stalk	KOH at 600 °C	761.89	3.5	This work
Cor cob	KOH at 600 °C	663.17	3.19	This work

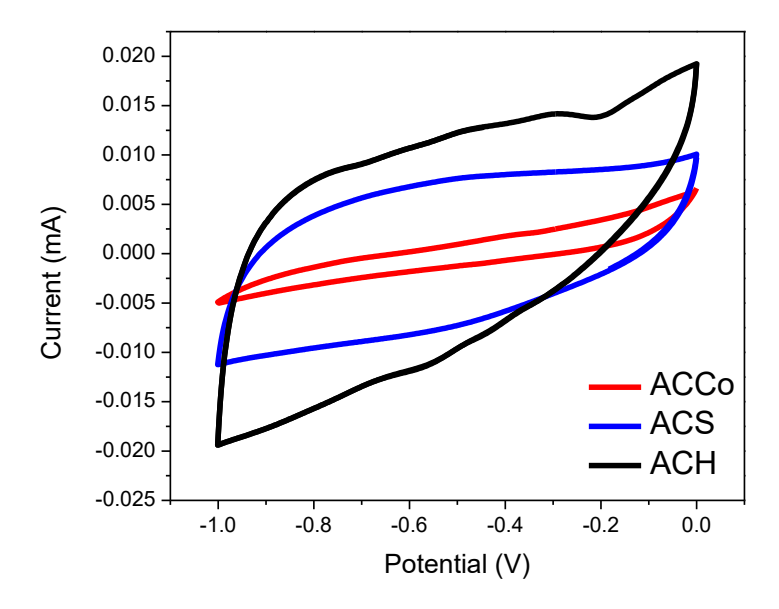


Fig 6. CV profiles of ACH, ACS and ACCo

to establish the fact that, given the kind of method employed in this study, AC with the best CO_2 capture performance can be obtained from CH. Corn stalk and CCo, though low, still display better CO_2 adsorption than AC sourced from starch and peanut shells (Table 3)

3.5. Electrochemical properties of electrodes

3.5.1. Cyclic voltammetry (CV) and Galvanostatic charge/discharge (GCD)

A three-electrode system performed CV and GCD analysis on ACH, ACS, and ACCo within a potential window -1 to 0 mV in 6 M KOH electrolyte. With a scan rate of 100 mV/s, it can be noticed from Figure 6 that all CV curves display quasi-rectangular shapes, which is indicative of capacitive performance. There also exist some broad peaks that affirm pseudo-capacitance contributions. The largest area under the CV curve exhibited by ACH implies it possesses the highest capacitance. In addition to the area, the well-ordering of structures has been confirmed to improve the specific capacitance of biomass–sourced ACs (Mehdi *et al.* 2023). The GCD plots of ACs derived from the selected corn stover at 0.5 A/g are shown in Figure 7a. Each curve is almost symmetric

with quasi-linear slopes, which is indicative of capacitive behavior. The largest loop area and the longest time for discharge are possessed by ACH; this shows that AC from CH displays the best capacitive ability. This is consistent with the CV results. The specific capacitances of ACH, ACS, and ACCo were determined at 0.5 A/g (Figure 7b). The highest specific capacitance (430 F/g) is displayed by ACH followed by 257.5 F/g in ACS and the least, 85 F/g characterized by ACCo. The best porous structure exhibited by ACH is responsible for its superlative performance. The capacitive performances of some ACs produced from other biomass in comparison with the ones synthesized in this study are shown in Table 4. At a decent current density ranging from 0.5 - 1.2 A/g, the relationship between ED and PD is represented by a Ragone plot shown in Figure 7c. The plot reveals that ACH electrode displays the best performance as it possesses its maximum ED (59.7 Wh/kg) at a PD value of 250 W/kg; this remains the highest of the three processed ACs.

3.5.2. Electrical double layer capacitive (EDLC) and pseudo capacitive (pseudo—C) contributions

To know the charge storage mechanism of ACH, ACS, and ACCo, Dunn and Trasatti methods were used. Both methods

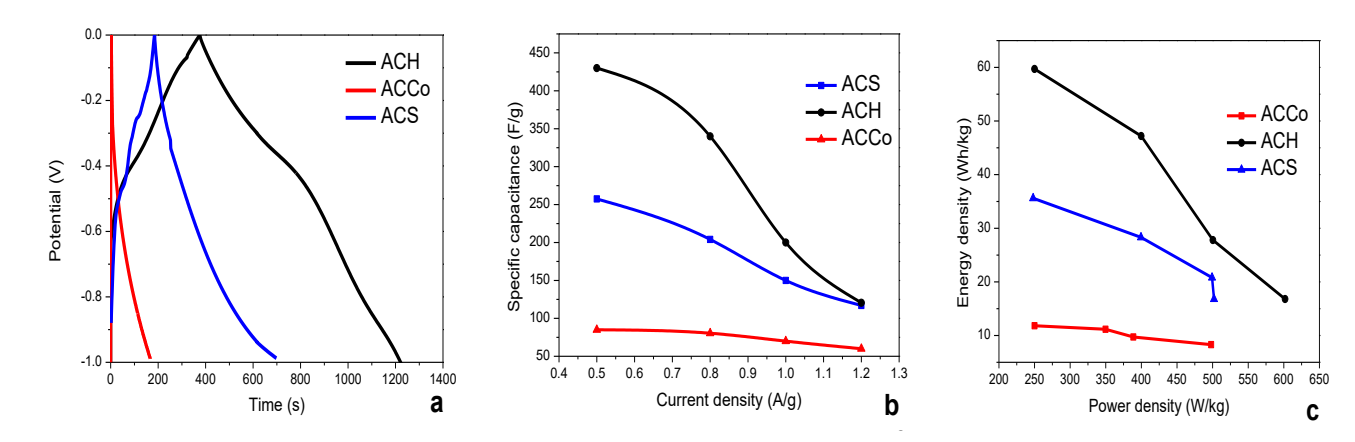


Fig 7. (a) GCD (b) specific capacitance (c) Ragone Plots of ACH, ACS and ACCo

Table 4Electrochemical performance comparisons of some ACs sourced from different biomass via pyrolysis and chemical activation method with ACs synthesized in this study.

Biomass	Activation agent	I_m (A/g)	C _p (F/g)	Electrolyte	Reference
Rose flower	KOH/KNO₃	1	350	6 M KOH	(Mehdi <i>et al. 2023</i>)
Tea leaf waste	KOH + H3PO4	0.5	131.95	3 M KOH	(Thirumal et al. 2022)
	Two-step KOH				
Lotus seedpods	activation	0.5	201.1	6 M KOH	(Wu et al. 2021)
Camphor tree grains	$CuCl_2$	1	423	6 M NaOH	(Hao, et al. 2024)
Enhydra fluctuant	KOH + NH₄Cl	1	428	0.5 M H_2SO_4	(Jalalah <i>et al.</i> 2021)
Polyalthia longifolia seeds	KOH	1	365	1M Na ₂ SO ₄	(Srinivasan et al. 2019)
Corn husk	KOH	0.5	430	6 M KOH	This work
Corn stalk	KOH	0.5	257.5	6 M KOH	This work

evaluated the capacitive (EDLC) and diffusive (pseudo-C) contributions to the total charge of each processed material. For the Dunn method, Equation (4) was used (Rajkumar *et al.* 2024).

$$i(v) = K_1 v + K_2 v^{\frac{1}{2}}$$
 (4)

From Equation (4), i(V) represents the output current; ν stands for scan rates; the capacitive and diffusive currents are represented by $K_1\nu$ and $K_2\nu^{\frac{1}{2}}$, respectively. The equation can be further simplified into:

$$\frac{i}{\frac{1}{\nu^{2}}} = K_{1}\nu^{\frac{1}{2}} + K_{2} \tag{5}$$

Output current was measured from the CV result of each AC at 10, 20, 30, 50 and 100 mV/s scan rates at a fixed applied potential (-0.3 V). The values of K_1 and K_2 were got from the plots of $\frac{1}{v^2}$ against $v^{\frac{1}{2}}$ (Figure 8a) and the capacitive and diffusive

currents were determined. At a selected scan rates of 30 mV/s,(Figure 8b),, applying Dunn method shows that capacity of each electrode is more influenced by diffusive contribution (Pseudo-C) as this occupies a more dominant percentage compared to the capacitive contribution.

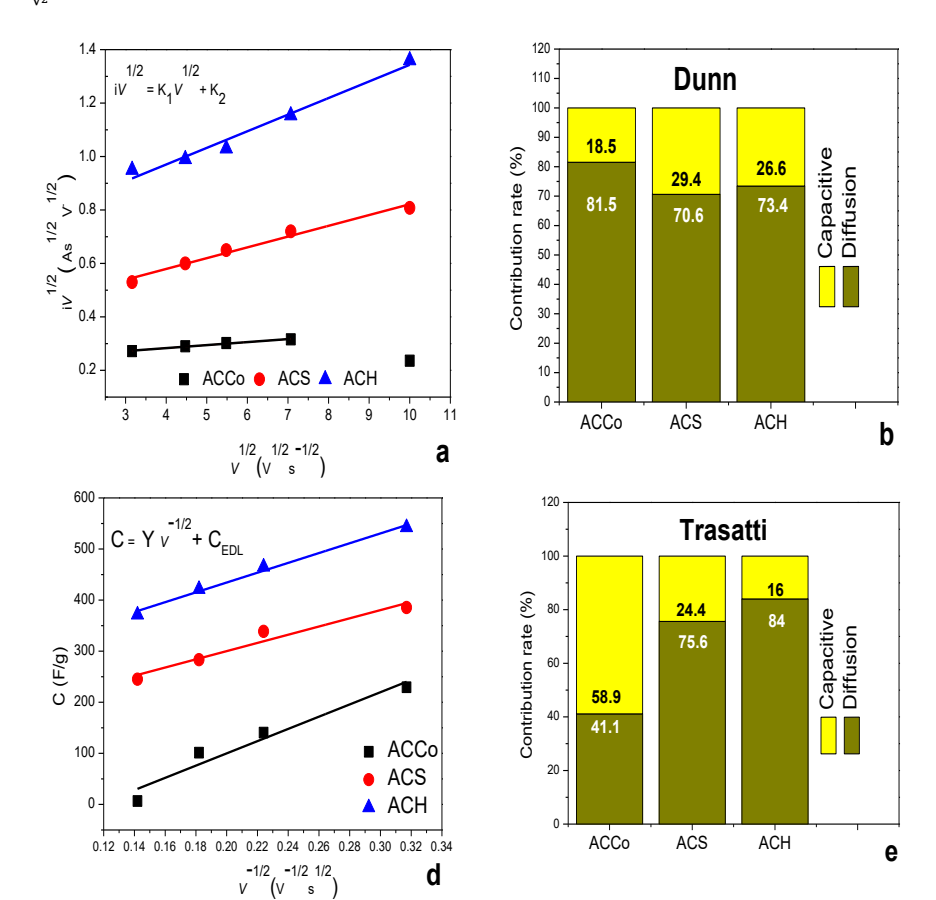
As regards the Trasatti method, equations (5), (6) and (7) were used (Jeloo *et al.* 2024).

$$C = \frac{S}{2m\Delta V_{\nu}} \tag{5}$$

$$C^{-1} = X \nu_2^{\frac{1}{2}} + C_T^{-1}$$
 (6)

$$C = Y \nu^{-\frac{1}{2}} + C_{EDL}$$
 (7)

Here, C represents the areal capacitance, which was calculated from the CV curves of each AC. The total capacitance is denoted by C_T , calculated from the linear fit of C^{-1} against $v^{\frac{1}{2}}$ graph



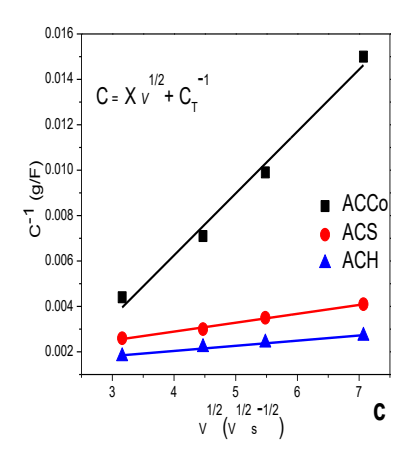


Fig 8. Analysis of pseudo-C and EDLC contributions for ACCo, ACS and ACH. Dunn method: (a) $\frac{1}{1}$ vs. $v^{\frac{1}{2}}$ linear plots for calculating the values of K_1 and K_2 (b) EDLC and pseudo-C fractions for electrodes at 30 mV/s. Trassatti method: (c) Plots C^{-1} vs. $v^{\frac{1}{2}}$ to evaluate C_T (d) Plots C against $v^{-\frac{1}{2}}$ to evaluate C_{EDL} (e) EDLC and pseudo-C fractions for electrodes at 30 mV/s.

according to equation (6) (the inverse of $C_{T^{-1}}$ gives the value of C_{T}); X and Y are constants (slope of each linear plot) while the EDLC contribution is represented by C_{EDL} . The relationship between pseudo and EDL capacitive contributions is given in equation:

$$C_{T} = C_{EDL} + C_{Pseudo}$$
 (8)

Figure 8c and d displays the C^{-1} against $v^{\frac{1}{2}}$ and C against $v^{-\frac{1}{2}}$ plots where the y-intercepts were C_{T}^{-1} and C_{EDL} . Trasatti method also shows that the capacity of each electrode is dominated by diffusive contribution, which is consistent with the Dunn method (Figure 8 e). Although the capacitive contribution seems greater than the diffusive contribution in ACCo electrode, the latter is still considerably high (41.1 %).

3.5.3. Electrochemical Impedance Spectroscopy (EIS)

properties each The charge transport electrode/electrolyte interface and the conductivity were analyzed using EIS. This is represented by the Nyquist and Bode plots shown in Figures 9 and 10. Both plots evaluate the frequency-dependent performance of each electrode/electrolyte system. Within the region of high frequency (Figure 9), there exists a semicircle-like curve, which connotes the charge transfer existing between the electrode/electrolyte interface; within this region, the solution resistance (R_S) was determined by extrapolating the curve along Z' – axis. The R_S is a measure of the refusal of ionic transfer in an electrolyte; when R_S is low, it means ionic flow through the electrolyte occurs with little hindrance. The equivalent series resistance (ESR) was measured from the total contact resistance that existed between the current collector electrode and the ohmic resistance of the electrode/electrolyte interface. The EIS determines the performance of supercapacitors in application; a low ESR value has been reported to impact good efficiency, slow degradation and reduced heat generation (Roh et al. 2025). The difference between the ESR and Rs is the charge transfer resistance (RCT). This resistance is a function of the opposition encountered by ions when they travel across the electrode/electrolyte interface in an electrochemical system. In this study, the EIS result shows that ACH possesses the least Rs, ESR, and R_{CT} (Table 5). This implies that ACH allows the fastest penetration (diffusion) of electrolyte ions into its surface, thereby promoting an active electrode/electrolyte interface. At low frequency regions, there exist straight lines that imply reductions in the electrode/electrolyte interface (the high

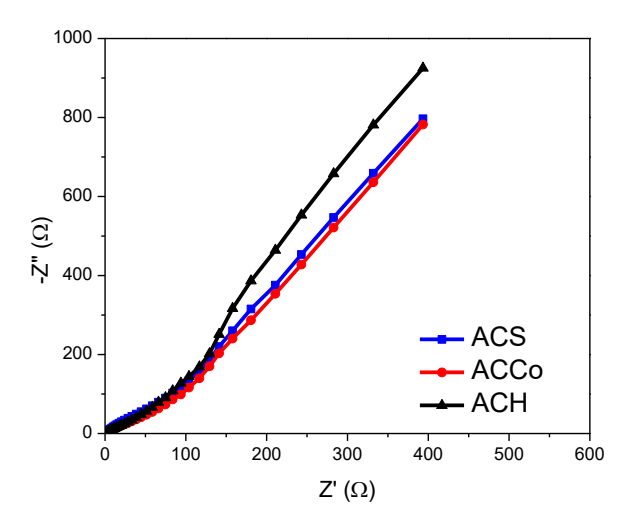


Fig 9. Nyquist plots for ACS, ACCo, and ACH

Table 5RCT, RS and ESR of ACH, ACS and ACCo from EIS analysis

ACs	$R_{CT}(\Omega)$	$R_{S}(\Omega)$	ESR (Ω)
ACH	1.9	0.42	2.32
ACS	2.03	0.46	2.49
ACCo	2.34	0.48	2.82

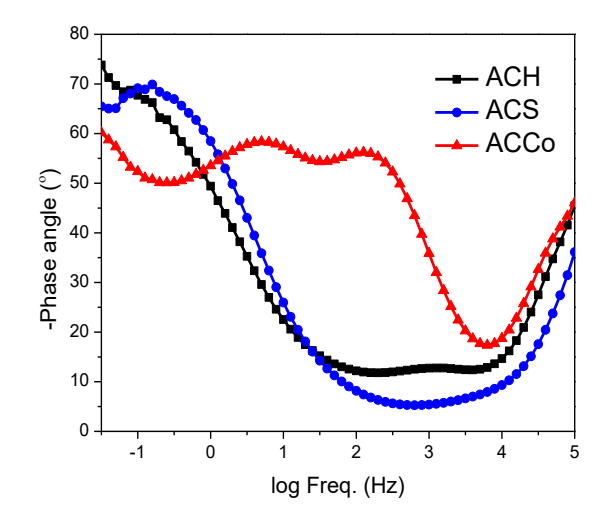


Fig 10. Bode plots for ACS, ACCo, and ACH

conductivity of electrodes beyond the semicircle-like curve eventually leads to this). The straight line that is nearest to the vertical is exhibited by ACH (compared to ACS and ACCo), suggesting that it displays the best capacitive behavior.

Bode plots showing phase angle–frequency relationships are displayed in Figure 10. The phase angle has been reported to be near 90° for a conventional capacitive material and very close to 45° for a pseudo capacitive material (Krishnamoorthy *et al.* 2014). Figure 10 shows that for the synthesized ACs, the phase angle (at the tail) ranges between 59.1 – 73.4° and this verifies that the capacitive nature of the AC-coated Ni foams is a combination of EDL and pseudo-capacitance. The high phase angle (73.4.°) at high frequency is observed in the plot of ACH, showing that it exemplifies the highest pseudo-capacitive performance by permitting the best electrolyte ion transport. The phase angles for ACS and ACCo are 66.1 and 59.1° respectively, which implies that ion transport in ACS is faster than that of ACCo.

5. Conclusion

In this study, biomass activated carbons (ACs) have been sourced from corn stover – the husk (ACH), stalk (ACS), and cob (ACCo). A two-stage pyrolysis, both at 600 °C, was employed (the second was combined with KOH activation). Although all synthesized ACs display a porous structure, findings show that corn husk (CH) possesses the best porous texture regarding surface area, size, and volume, followed by corn stalk (CS). At 273 K and 0.95 bar, the highest amount of CO₂ (4.63 mmolg⁻¹) is captured by ACS and the least CO₂ capture capacity of 3.19 mmolg⁻¹ is exhibited by ACCo. The huge micropore surface area and size of ACH observed from SEM and N₂ BET analyses are

responsible for its best electrochemical properties; the maximum specific capacitance (430 F/g) at 0.5 A/g current density. Dunn and Trasatti methods show that the capacity of each electrode is more influenced by the diffusive contribution. The highest phase angle (73.4.º) recorded in the Bode plot for ACH shows that it permits the best electrolyte ion transport; this is also justified by the EIS resul,t which confirms that the electrode displays the fastest diffusion of electrolyte ions into its surface. Although the reason why CH performs best among the three corn stover is not established, this study is quite important in the sense that it sets a foundation for our future studies where complex activation techniques (including parameters and diverse characterizations) will be devised on these three stover to arrive at scientific mechanisms and in turn, the best optimal approach for their applications for energy storage.

Acknowledgments

The electrochemical studies were successfully performed at the Surface Engineering Research Laboratory (SERL), department of Chemical, Metallurgical & Materials Engineering, Tshwane University of Technology, Pretoria – South Africa.

References

- Ahmed, M.B., Johir, M.A.H., Zhou, J.L., Ngo, H.H., Nghiem, L.D., Richardson, C., Moni, M.A., & Bryant, M.R. (2019). Activated Carbon Preparation from Biomass Feedstock: Clean Production and Carbon Dioxide Adsorption. *Journal of Cleaner Production*, 225, 405-413; https://doi.org/10.1016/j.jclepro.2019.03.342
- Alabadi, A., Razzaque, S., Yang, Y., Chen, S., & Tan, B. (2015). Highly Porous Activated Carbon Materials from Carbonized Biomass with High CO2 Capturing Capacity. *Chemical Engineering Journal*, 281, 606-612; https://doi.org/10.1016/j.cej.2015.06.032
- Alauddin, Z.A.B.Z., Lahijani, P., Mohammadi, M., & Abdul Rahman, M. (2010). Gassification of Lignocellulosic Biomass in Fluidized Beds for Renewable Energy Development: A Review. *Renewable and Sustainable Energy Reviews*, 14(9), 2852-2862; https://doi.org/10.1016/j.rser.2010.07.026
- Awasthi, G.P., Bhattarai, D.P., Maharjan, B., Kim, K.S., Park, C.H., & Kim, C.S. (2019). Synthesis and Characterizations of Activated Carbons from Wisteria Sinensis Seed Biomass for Energy Storage Appications. *Journal of Industrial and Engineering Chemistry*, 72, 265-272; https://doi.org/10.1016/j.jiec.2018.12.027
- Blasi, C.D.(2009). Combustion and Gasification Rates of Lignocellulosic Chars. *Progress in Energy and Combustion Science*, 35,(2), 121-140; https://doi.org/10.1016/j.pecs.2008.08.001
- Chen, F., Juan, Y., Bai, T., Long, B., & Zhou, X. (2016). Facile Synthesis of Few-Layer Graphene from Biomass Waste and its Application in Lithium Ion Batteries. *Journal of Electroanalytical Chemistry*, 768, 18-26; https://doi.org/10.1016/j.jelechem.2016.02.035
- Cao, Y., Wang, K., Wang, X., Gu, Z., Fan, Q., Gibbons, W.R., Hoefelmeyer, J.D., Kharel, P.R., & Shrestha, M. (2016). Hierarchical Porous Activated Carbon for Supercapacitor Derived from Corn Stalk Core by Potassium Hydroxide Activation. *Electrochimica Acta*, 212, 839-847; https://doi.org/10.1016/j.electacta.2016.07.069
- Carmen, B., & Blasi, C.D. (2013). A Unified Mechanism of the Combustion Reactions of Lignocellulosic Fuels. *Thermochimica Acta*, 565(10), 58-64; https://doi.org/10.1016/j.tca.2013.04.014
- Dhineshkumar, S., Rajkumar, S., Sathiyan, A., & Merlin, J.P. (2024). Fabrication of Ag2WO4/PANI Composite with Enhanced Supercapacitor Performance. *Journal of Materials Science: Materials in Electronics*, 35, 1409, 1-15; https://doi.org/10.1007/s10854-024-13202-2
- Fagbayigbo, B.O., Opeolu, B.O., Fatoki, O.S., Akenga, T.A. & Olatunji, O.S. (2017). Removal of PFOA and PFOS from Aqueous Solutions using Activated Carbon Produced from Vitis Vinifera Leaf Litte.

- Environmental Science Pollution Research, 24, 13107–13120; https://doi.org/10.1007/s11356-017-8912-x
- Fonts, I., Martínez, M.A., Carstensen, H.H., Benés, M., Pires, A.P.P., Perez, M.G., & Bilbao, P. (2021). Thermodynamic and Physical Property Estimation of Compounds Derived from the Fast Pyrolysis of Lignocellulosic Materials. *Energy and Fuels*, 21, 17114–17137;https://pubs.acs.org/doi/10.1021/acs.energyfuels.1c0170
- Gan, Y.X. (2021). Activated Carbon from Biomass Sustainable Sources.

 C. Journal of Carbon Research, 7(2), 1-33; https://doi.org/10.3390/c7020039
- Garcia, E.H., Riojas, A.A.C., Monje, I.E., López, E.O., Pinedo, O.M.A., Planes, G.A., & Moncada, A.M.B. (2024). Activated Carbon Electrodes for Supercapacitors from Purple Corncob (*Zea mays L.*). *ACS Environmental Au*, 4(2), 80-88; https://doi.org/10.1021/acsenvironau.3c00048
- Gbenebor, O.P., Olanrewaju, O.A., Usman, M.A. & Adeosun, S.O. (2023). Lignin from Brewers' Spent Grain: Structural and Thermal Evaluations. *Polymers*, 13(10), 1-14; https://doi.org/10.3390/polym15102346
- González, D.L., Lopez, M.F., Valverde, J.L. & Silva, L.S. (2014). Gasification of Lignocellulosic Biomass Char Obtained from Pyrolysis: Kinetic and Evolved Gas Analyses. *Energy*, 71(15), 456-467; https://doi.org/10.1016/j.energy.2014.04.105
- Hashemi, B., Sarker, S., Lamb, J.J., & Myklebust, L.K. (2021). Yield Improvements in Anaerobic Digestion of Lignocellulosic Feedstocks. *Journal of Cleaner Production*, 288, 1-27; https://doi.org/10.1016/j.jclepro.2020.125447
- Hao, J., Wang, B., Du, J., Wu, C., Qin, W., & Wu, X. (2024). Interfacial Regulation of Biomass-Derived Carbon Towards High-Performance Supercapacitor. *Journal of Energy Storage*, 86, 1-10; https://doi.org/10.1016/j.est.2024.111301
- Hepsiba P., Rajkumar, S., Elanthamilan, E., Wang, S.F., & Merlin, J.P. (2022). Biomass-Derived Porous Activated Carbon from Anacardium Occidentale Shell as Electrode Material for Supercapacitors. New Journal of Chemistry, 46, 8863 8873; https://doi.org/10.1039/D2NJ01041K
- Igathinathane, C., Womac, A.R., & Sokhansanj, S. (2010). Corn Stalk Orientation Effect on Mechanical Cutting. *Biosystems Engineering*, 107, 97 -106; https://doi.org/10.1016/j.biosystemseng.2010.07.005
- Igathinathane, C., Womac, A.R., Sokhansanj, S., & Pordesimo, L.O. (2006), Mass and Moisture Distribution in Aboveground Components of Standing Corn Plants. *Transactions of the ASABE*, 49(1), 97-106; https://doi.org/10.13031/2013.20217) @2006
- Jalalah, M., Han, H., Mahadani, M., Nayak, A.K., & Harraz, F.A. (2023).
 Novel Interconnected Hierarchical Porous Carbon Derived from Biomass for Enhanced Supercapacitor Application. *Journal of Electroanalytical Chemistry*, 935, 1-9; https://doi.org/10.1016/j.jelechem.2023.117355
- Jeloo, Z.A.G., Ghasemzadeh, S., Hosseini-Monfared, H., Javanbakht, M., Naji, L., Najaflo, M., & Hamidi, S. (2024). From Barley Straw Biomass to N/S Co-Doped as Electrode Material for High-Performance Supercapacitor Applications, *Materials Chemistry and Physics*, 323, 1-14; https://doi.org/10.1016/j.matchemphys.2024.129653
- Kamperidou, V., & Terzopoulou, P. (2021). Anaerobic Digestion of Lignocellulosic Waste Materials. *Sustainability*, *13*(22), 1-23; https://doi.org/10.3390/su132212810
- Karnan, M., Subramani, K., Srividhya, P.K., & Sathish, M. (2017). Electrochemical Studies on Corncob Derived Activated Porous Carbon for Supercapacitors Application in Aqueous and Nonaqueous Electrolytes. Electrochimica Acta, 228, 586-596; https://doi.org/10.1016/j.electacta.2017.01.095
- Krishnamoorthy, K., Veerasubramani, K.G., Radhakrishnan, S., & Kim, S.J. (2014). Supercapacitive Properties of Hydrothermally Synthesized Sphere like MoS2 Nanostructures. *Materials Research Bulletin*, 50, 499-502: https://doi.org/10.1016/j.materresbull.2013.11.019
- Kwapinski, W., Byrne, C.M.P., Kryachko, E., Wolfram, P., Adley, C., Novotny, E.H., & Hayes, M.H.B. (2010). Biochar from Biomass and

- Waste. Waste and Biomass Valorization, 1, 177–189; https://doi.org/10.1007/s12649-010-9024-8
- Li, Y., Li, C., Qi, H., Yu, K., & Liang, C. (2018). Mesoporous Activated Carbon from Corn Stalk Core for Lithium Ion Batteries. *Chemical Physics*, 506, 10–16; https://doi.org/10.1016/j.chemphys.2018.03.027
- Luo, Z., Cal, P.L.D., Chen, Q., Qin, P., Tan, T., & Cao, H. (2017). Comparison of Performances of Corn Fiber Plastic Composites Made from Different Parts of Corn Stalk. *Industrial Crops and Products*, 95, 521-527; https://doi.org/10.1016/j.indcrop.2016.11.005
- Mehdi, R., Naqvi, S.R., Khoja, A.F., & Hussain R. (2023). Biomass Derived Activated Carbon by Chemical Surface Modification as a Source of Clean Energy for Supercapacitor Application. *Fuel*, 348, 1-10; https://doi.org/10.1016/j.fuel.2023.128529
- Mopoung, S., & Dejang, N. (2021). Activated Carbon Preparation from Eucalyptus Wood Chips using Continuous Carbonization–Steam Activation Process in a Batch Intermittent Rotary Kiln. *Scientific Reports*, 11(13948), 1-9; https://doi.org/10.1038/s41598-021-93249-x
- Mumtaz, H., Farhan, M., Amjad, M., Riaz, F., Kazim, A.H., Sultan, M., Farooq, M., Mujtaba, M.A., Hussain, I., Imran, M., Anwar, S., El-Sherbeeny, A.M., Siddique, F.A., Armaković, S., Ali, Q., Chaudhry, I.A., & Pettinau, A. (2021). Biomass Waste Utilization for Adsorbent Preparation in CO2 Capture and Sustainable Environment Applications. Sustainable Energy Technologies and Assessments, 46, 1-8; https://doi.org/10.1016/j.seta.2021.101288
- Oliva, A., Tan, L.C., Papirio, S., Esposito, G., & Lens, P.N.L. (2021). Effect of Methanol-organosolv Pretreatment on Anaerobic Digestion of Lignocellulosic Materials. *Renewable Energy*, 169, 1000-1012; https://doi.org/10.1016/j.renene.2020.12.095
- Olivares, R.D.O., Peralta, D.R.L., Arias, D.M., Okolie, J.A., Gallegos, A.K.C., Sebastian, P.J., Mayer, A.R., & Okoye, P.U. (2022). Production of Nanoarchitectonics Corncob Activated Carbon as Electrode Material for Enhanced Supercapacitor Performance. *Journal of Energy Storage*, 55, 1-12; https://doi.org/10.1016/j.est.2022.105447
- Omoriyekomwan, J.E., Tahmasebi, A., Dou, J.J., Wang, R., & Yu, J. (2021). A Review on the Recent Advances in the Production of Carbon Nanotubes and Carbon Nanofibers via Microwave-Assisted Pyrolysis of Biomass. Fuel Processing Technology, 214, 1-22; https://doi.org/10.1016/j.fuproc.2020.106686
- Peralta, D.R.L., Brito, E.D., Orugba, H.O., Arias, D.M., Gallegos, A.K.C., Okolie, J.A., & Okoye, P.U. (2023). Sponge-like Nanoporous Activated Carbon from Corn Husk as a Sustainable and Highly Stable Supercapacitor Electrode for Energy Storage. *Diamond and Related Materials*, 138, 1-13; https://doi.org/10.1016/j.diamond.2023.110176
- Pu, Q., Zou, J., Wang, J., Lu, S., Ning, P., Huang, L., & Wang, Q. (2021). Systematic Study of Dynamic CO2 Adsorption on Activated Carbons Derived from Different Biomass. *Journal of Alloys and Compounds*, 887, 1-14; https://doi.org/10.1016/j.jallcom.2021.161406
- Rajkumar, S., Gowri, S., Karthikeyan, M., Dhineshkumar, S., Ansar, S., Priyadharshan, M., & Merlin, J.P. (2024). One-step Synthesis of Nanostructured Ag2Mo2O7 with Enhanced Efficiency for Supercapacitors. *Ionics*, 1-13; https://doi.org/10.1007/s11581-024-05755-3
- Rajkumar, S., Karthikeyan, M., Manohar, A., Dhineshkumar, S., & Merlin, J.P. (2024). One-Step Synthesis and Fabrication of ZrMo2O8 Nanostructures as Advanced Electrode Material for Energy Storage Applications. *Journal of Industrial and Engineering Chemistry*, 137, 162-173; https://doi.org/10.1016/j.jiec.2024.03.002
- Rahmati, S., Doherty, W., Dubal, D., Atanda, L., Moghaddam, L., Sonar, P., Hessel, V., & Ostrikov, K. (2020). Pretreatment and Fermentation of Lignocellulosic Biomass: Reaction Mechanisms and Process Engineering. *Reaction Chemistry & Engineering*, 5, 2017-2047; https://doi.org/10.1039/D0RE00241K
- Rani, M.U., Nanaji, K., Rao, T.N., & Deshpande, A.S. (2020). Corn Husk Derived Activated Carbon with Enhanced Electrochemical Performance for High-Voltage Supercapacitors. *Journal of Power*

- Sources, 471, 1-10; https://doi.org/10.1016/j.jpowsour.2020.228387
- Reddy, N., & Yang, Y., (2015). Natural Cellulose Fibers from Corn Stover. Innovative Biofibers from Renewable Resources. Springer Berlin Heidelberg, 5–8; https://doi.org/10.1007/97
 Reddygunta, KKR., Beresford, R., Šiller, L., Berlouis, L. & Ivaturi, A.
- Reddygunta, KKR., Beresford, R., Šiller, L., Berlouis, L. & Ivaturi, A. (2023). Activated Carbon Utilization from Corn Derivatives for High-Energy-Density Flexible Supercapacitors. *Energy Fuels*, 37,19248–19265; https://doi.org/10.1021/acs.energyfuels.3c01925
- Roh, C, Jeon, H, Kim, S, Kim, J, Song S, Lee, L, & Kang, S. (2025). A Study on Equivalent Series Resistance Estimation Compensation for DC-Link Capacitor Life Diagnosis of Propulsion Drive in Electric Propulsion Ship. *Processes*, 13(2), 1-18; https://doi.org/10.3390/pr13020291
- Senneca, O., & Cerciello, F. (2023). Kinetics of Combustion of Lignocellulosic Biomass: Recent Research and critical issues, *Fuel*, 347, 1-16: https://doi.org/10.1016/j.fuel.2023.128310
- Serafin, J., Baca, M., Biegun, M., Mijowska, E., Kaleńczuk, R.J., Nazzal, J.S., & Michalkiewicz, B. (2019). Direct Conversion of Biomass to Nanoporous Activated Biocarbons for High CO2 Adsorption and Supercapacitor Applications. *Applied Surface Science*, 497, 1-19; https://doi.org/10.1016/j.apsusc.2019.143722
- Serafin, J., Narkiewicz, U., Morawski, A.W., Wrobel, R.J., & Michalkiewicz, B. (2017). Highly Microporous Activated Carbons from Biomass for CO2 Capture and Effective Micropores at Different Conditions. *Journal of CO2 Utilization*, 18, 73-79; https://doi.org/10.1016/j.jcou.2017.01.006
- Singh, G., Kim, I.Y., Lakhi, K.S., Srivastava, P., Naidu, R., & Vinu, A. (2017). Single Step Synthesis of Activated Bio-Carbons with A High Surface Area and their Excellent CO2 Adsorption Capacity. Carbon, 116, 448-455; https://doi.org/10.1016/j.carbon.2017.02.015
- Srinivasan, R., Elaiyappillai, E., Pandian, H.P., Vengudusamy, R., Johnson, P.M., Chen, S.M., & Karvembu, R. (2019). Sustainable Porous Activated Carbon from *Polyalthia Longifolia* Seeds as Electrode Material for Supercapacitor Application. *Journal of Electroanalytical Chemistry*, 849, 1-12; https://doi.org/10.1016/j.jelechem.2019.113382
- Surya, K., & Michael, M.S. (2020). Novel Interconnected Hierarchical Porous Carbon Electrodes Derived ffom Bio-waste of Corn Husk for Supercapacitor Applications. *Journal of Electroanalytical Chemistry*, 878, 1-10; https://doi.org/10.1016/j.jelechem.2020.114674
- Thirumal, V., Yuvakkumar, R., Ravi, G., Dineshkumar, G., Ganesan, M., Alotaibi, S.H., & Velauthapillai, D. (2022). Characterization of Activated Biomass Carbon from Tea Leaf for Supercapacitor Applications. *Chemosphere*, 291, 1-8; https://doi.org/10.1016/j.chemosphere.2021.132931
- Tounsadi, H., Khalidi, A., Abdennouri, M., & Barka, N. (2016). Activated Carbon from Diplotaxis Haria Biomass: Optimization from Preparation Conditions and Heavy Metal Removal. *Journal of the Taiwan Institue of Chemical Engineers*, 59, 348-358; https://doi.org/10.1016/j.jtice.2015.08.014
- Vinayagam, M., Babu, R.S., Sivasamy, A., & Ferreira de Barros, L.A. (2020). Biomass-Derived Porous Activated Carbon from Syzygium Cumini Fruit Shells and Dhrysopogon Zizanioides Roots for High-Energy Density Symmetric Supercapacitors. *Biomass and Bioenergy*, 143, 1-8; https://doi.org/10.1016/j.biombioe.2020.105838
- Vinayagam, M., Babu, R.S., Sivasamy1, A., & Ferreira de Barro, A.L. (2021). Biomass-Derived Porous Activated Carbon Nanofbers from Sapindus Trifoliatus Nut Shells for High-Performance Symmetric Supercapacitor Applications. *Carbon Letters*, 31, 1133-1143; https://doi.org/10.1007/s42823-021-00235-4
- Vinayagam, M., Babu, R.S., Sivasamy1, A., & Ferreira de Barro, A.L. (2024). Physical Activation Assisted Porous Activated Carbon from Strychnos Potatorum Shells for High-Performance Symmetric Supercapacitors. Materials Letters, 371, 1-4; https://doi.org/10.1016/j.matlet.2024.136961
- Wu, L., Cai, Y., Wang, S., & Li, Z. (2021). Doping of Nitrogen into Biomass-Derived Porous Carbon with Large Surface Area using N2 Non-Thermal Plasma Technique for High-Performance

- Supercapacitor. *International Journal of Hydrogen Energy*, 46(2), 2432-2444: https://doi.org/10.1016/j.ijhydene.2020.10.037
- Xiang, J., Zheng, H., Xue, H., Huang, W., Yuan, P., Yang, T., Yang, L., Wang, Q., & Zhang, Y. (2024). Performance Study of High Energy Storage Supercapacitor from Waste Corn Husk Biomass Electrode Materials. *Journal of Physics and Chemistry of Solids*, 194, 1-12; https://doi.org/10.1016/j.jpcs.2024.112265
- Yu, K., Zhu, H., Qi, H., & Liang, C. (2018). High Surface Area Carbon Materials Derived from Corn Stalk Core as Electrode for Supercapacitor. *Diamond and Related Materials*, 88, 18-22; https://doi.org/10.1016/j.diamond.2018.06.018
- Yu, S., Wang, L., Li, Q., Zhang, Y., & Zhou, Z. (2022). Sustainable Carbon Materials from the Pyrolysis of Lignocellulosic Biomass. *Materials*

- *Today Sustainability*, 19, 1-12; https://doi.org/10.1016/j.mtsust.2022.100209
- Zeng, K., He, X., Yang, H., Wang, X., & Chen, H. (2019). The Effect of Combined Pretreatments on the Pyrolysis of Corn Stalk. Bioresource Technology, 281, 309-317; https://doi.org/10.1016/j.biortech.2019.02.107
- Zhao, J., Yu, L., Ma, H., Zhou, F., Yang, K., & Wu, G. (2020). Corn Stalk-Based Activated Carbon Synthesized by a Novel Activation Method for High-Performance Adsorption of Hexavalent Chromium in Aqueous Solutions. *Journal of Colloid and Interface Science*, 578,650–659; https://doi.org/10.1016/j.jcis.2020.06.031



© 2025. The Author(s). This article is an open access article distributed under the terms and conditions of the Creative Commons Attribution-ShareAlike 4.0 (CC BY-SA) International License (http://creativecommons.org/licenses/by-sa/4.0/)